REPORT DOCUMENTATION PAGE

AFRL-SR-AR-TR-02-

0190

1. REPORT DATE *(DD-MM-YYYY)*	2. REPORT TYPE	3. DATES COVERED
23-05-2002	Final Technical	01/06/1999 - 30/11/2001

4. TITLE AND SUBTITLE
Coherent Beacon System for TechSat21 Science and Engineering

5a. CONTRACT NUMBER
F49620-99-C-0029

5b. GRANT NUMBER

5c. PROGRAM ELEMENT NUMBER

6. AUTHOR(S)
Robert C. Livingston

5d. PROJECT NUMBER

5e. TASK NUMBER

5f. WORK UNIT NUMBER

7. PERFORMING ORGANIZATION NAME(S) AND ADDRESS(ES)

Scion Associates, Inc.
439 Fillmore Street
Port Townsend, WA 983689

8. PERFORMING ORGANIZATION REPORT NUMBER
F49620-99-C-0029

9. SPONSORING / MONITORING AGENCY NAME(S) AND ADDRESS(ES)
AFOSR
801 N.Randolph St.
Room 732
Arlington VA 22203-1977

10. SPONSOR/MONITOR'S ACRONYM(S)

11. SPONSOR/MONITOR'S REPORT NUMBER(S)

12. DISTRIBUTION / AVAILABILITY STATEMENT

Approved for public release, distribution unlimited

20020614 174

13. SUPPLEMENTARY NOTES

14. ABSTRACT

A coherent radio beacon system has been designed that addresses the scientific, engineering and operational needs of the TechSat21 distributed aperture Space Based Radar (SBR). Had the program gone ahead, the beacon would have functioned as an unambiguous diagnostic of ionospheric effects for comparison to SBR performance. The cumulative beacon observations would have also provided the detailed statistical characterization of the radar channel that is required for development of SBR operational and mitigation strategies. As a scientific resource, beacons installed on multiple satellites of the TechSat21 cluster would have been able to separate, for the first time, the spatial and temporal variations in ionospheric structure.

The engineering and scientific design rationale is outlined, antenna options are discussed, and a high-accuracy, beacon-based cluster ranging system is described.

15. SUBJECT TERMS

16. SECURITY CLASSIFICATION OF:			17. LIMITATION OF ABSTRACT	18. NUMBER OF PAGES	19a. NAME OF RESPONSIBLE PERSON
unclassified					Robert C. Livingston
a. REPORT	b. ABSTRACT	c. THIS PAGE		39	19b. TELEPHONE NUMBER *(include area code)* (360) 379-4681

Final Technical Report, May 2002
Covering the Period 1 June 1999 to 31 November 2001

Coherent Beacon System for TechSat21 Science and Engineering

Prepared by:

Robert C. Livingston
Scion Associates
439 Fillmore Street
Port Townsend, Washington 98368

Prepared for:

Major Paul Bellaire
Air Force Office of Scientific Research
801 North Randolph Street
Arlington, Virginia 22203-1977

Contract F49620-99-C-0029

Summary

Under this contract Scion Associates initiated the development of a coherent radio beacon system that addresses the scientific, engineering and operational needs of the TechSat21 distributed aperture Space Based Radar (SBR). The beacon was designed to function as an unambiguous diagnostic of ionospheric effects for comparison to SBR performance. The cumulative beacon observations would have provided the detailed statistical characterization of the radar channel that is required for development of SBR operational and mitigation strategies. As a scientific resource, beacons installed on multiple satellites of the TechSat21 cluster would be able to separate, for the first time, the spatial and temporal variations in ionospheric structure. A powerful and practical adjunct to multi-beacon deployment would have been a precise ranging scheme for satellite cluster positioning.

Unfortunately, the TechSat system management decided that any scientific-oriented packages (such as the beacon) would not be installed on the spacecraft, and dropped that aspect of the program development. At that point, Scion Associates suspended spending on this contract. The primary reason was that any deliverable prototype, built for the specific and stringent demands of the TechSat platform, would not necessarily be applicable to other programs. Thus, spending on the program was limited to approximately 15% of the contract award total.

The first-order design decisions for the beacon system were accomplished early in the program. Those included design choices that could be made prior to any detailed specification of the TechSat21 spacecraft bus, frequency allocations and EMI requirements. For example, a nominal transmission spectrum of the beacon was established to satisfy the scientific and engineering goals of the program. This included a reference carrier at S-band, rather than at X-band, to reduce hardware complexity and to improve system phase noise performance. A variety of antenna designs were reviewed in some detail, keeping in mind the limited space available, and the need for good performance to support the broadband carrier transmissions used to measurement of total electron content (TEC).

In this final report, we briefly summarize the work done on three important aspects of the beacon design:

1. the transmitted spectrum of the beacon,
2. antenna options available for TechSat, and
3. a modeling test of the coherent beacon ranging scheme.

Rationale for the TechSat Beacon

A coherent beacon system aboard the TechSat21 satellites was designed to provide the following:

1) a unique opportunity to separate the temporal and spatial variations in the ionosphere.

2) an operational performance diagnostic that would provide a direct and unambiguous measure of ionospheric structure along the one-way radar channel.

3) a means to provide a database of engineering information about the ionospheric propagation channel collected during space-based radar (SBR) operations.

4) a source of accurate and detailed measurement of total electron content (TEC) across the SBR path.

The ionospheric information provided by a phase-coherent beacon is derived from the carrier signal phase received on the ground. The coherence of the beacon spectrum means that the geometrical phase due to the satellite motion can be removed exactly, leaving only the integrated effect of the ionospheric plasma along the path. Thus, it is possible to obtain a high-resolution measure of the change in TEC (ΔTEC), even when the geometrical Doppler shift is high.

The ionosphere always displays a wide spectrum of "structure". This includes long tidal scales (>100 km) down through short instability-generated irregularities (<500 m), and a whole zoo of structures in between. As the satellite borne beacon moves in time, the phase time series traces out an integrated replica of that structure that scales directly to ΔTEC.

At the carrier frequencies (> VHF) and scatter levels (weak to moderate) of interest, the phase of a transionospheric carrier scales with frequency as f^{-1}. For TechSat21, we planned to use a low measurement carrier at 800 MHz, and the analysis below shows that a measurement resolution of ~3° can be obtained at this frequency. This corresponds to a ΔTEC change of about 1×10^{13} electrons/m^2 along the propagation path, or a phase change of 0.25° at the 10 GHz SBR frequency. This sensitive and high-resolution measure of ΔTEC is one reason that the beacon could have benefited the evaluation of TechSat SBR operations.

As an illustration of the application, we can use data from the Wideband satellite that carried a coherent beacon between 1976 and 1978. Its lowest measurement carrier was at 137 MHz, and the data from a portion of a daytime typical pass at Stanford, California, is shown in the top frame of Figure 1. The overall shape of the ΔTEC variation is due to the geometry (approximately the secant of the elevation angle), although this particular day did show some north-south asymmetry in TEC. The phase record appears to be smooth, but actually contains significant structure. The phase perturbations, derived by filtering the ΔTEC record, are the second frame of the figure; this has been scaled per the pass

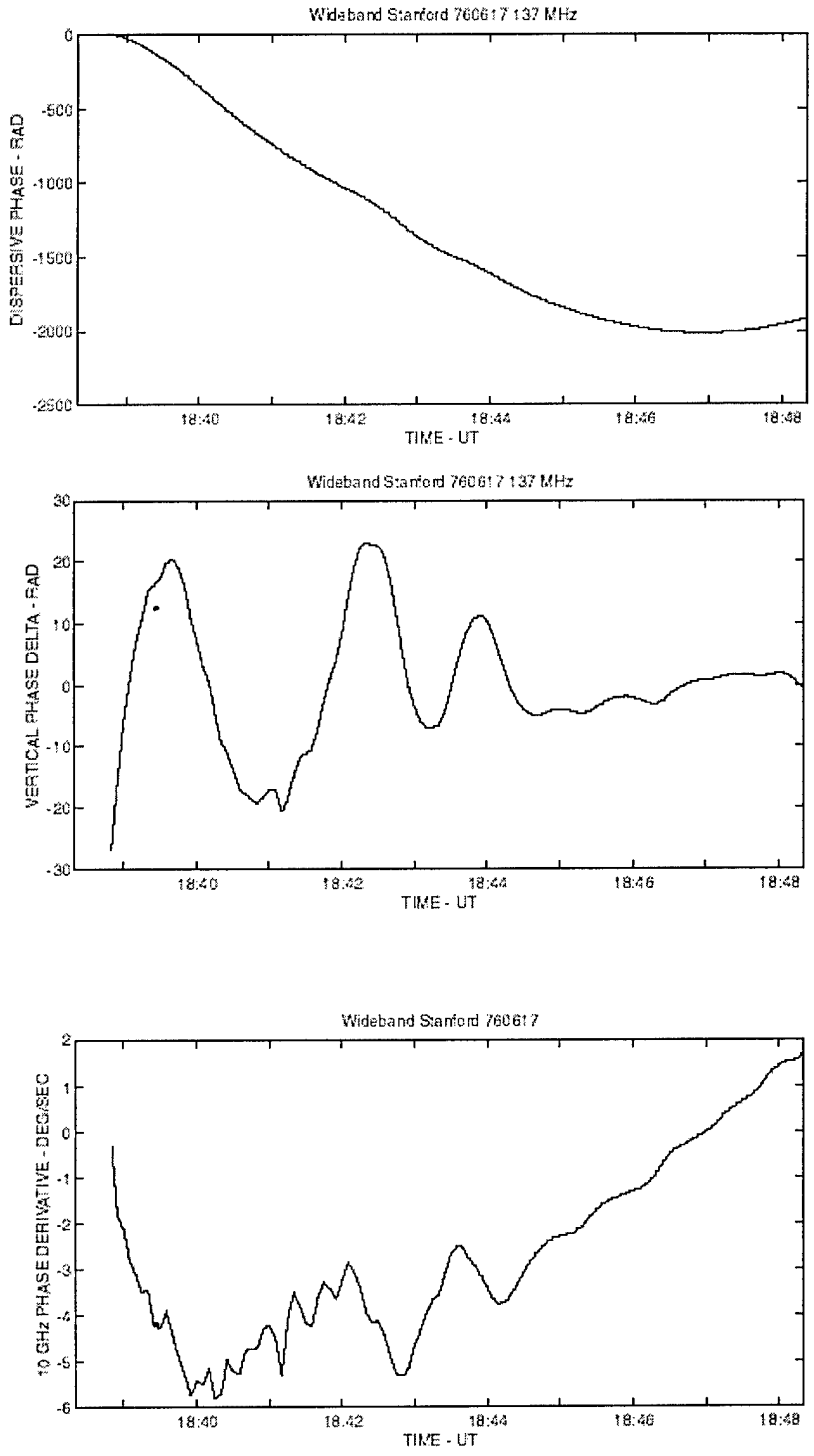

Figure 1. Wideband satellite data collected at Stanford, California.

geometry to correspond to an equivalent vertical change of phase. The phase delta scales as f^{-1} so the corresponding axis at the 10 GHz SBR frequency would be about ±0.4 radians. A more informative display, in the third frame of the figure, is the time derivative of phase that the radar would encounter. That exceeds several degrees per second at the radar operating frequency throughout a good portion of the pass.

The data in Figure 1 are a good illustration of what a TechSat21 radar would routinely encounter at mid-latitudes. The quantitative effect that similar structure would have on SBR performance depends upon the radar mode, of course. Coherent gain would be hampered to some degree, even with quadratic correction. What is important to note is:

1) The data set shown is quite typical of the daytime, mid-latitude ionosphere, and weak structure, like that shown, is more the norm than an exception.

2) a beacon is the only way that the presence of structure can be unambiguously determined. Other measurements (e.g. onboard dual-frequency GPS) cannot identify small perturbations.

Accordingly, if structure of this strength is likely to be a concern for TechSat performance, the beacon would have been an important adjunct for the evaluation of TechSat21 cluster SBR operations.

Beacon Spectrum Design

The basic observation goal of the beacon system can be stated simply: a high-accuracy measurement of the dispersive phase imparted to the signal by the ionosphere. More specifically, we would strive to measure total electron content (TEC), and changes in the total content (ΔTEC) along the signal path to an accuracy of 5×10^{13} electrons/m^2. It should be noted that the measurement includes the full dispersive phase spectrum, from bulk TEC through small ionospheric irregularity scales. At the carrier frequencies (> VHF) and scatter levels (weak to moderate) of interest, the phase of a transionospheric carrier scales with frequency as f^{-1}, so this ΔTEC resolution corresponds to ~25° dispersive phase change at 100 MHz, ~2.5° at 1000 MHz and ~0.25° at the 10 GHz SBR frequency.

The beacon technique utilizes a spectrum of harmonically related carriers that are phase coherent at the satellite beacon transmitter. The highest frequency is least affected by the ionosphere, and is received and divided down to provide a phase reference for the lower frequency carriers. When this is done, the phase each lower carrier becomes the difference of the two:

$$\phi_c - \frac{\phi_{ref}}{n} = -\frac{2\pi R}{c}\left[f_c - \frac{f_{ref}}{n}\right] + \kappa N_T\left[\frac{1}{f_c} - \frac{n}{f_{ref}}\right] \qquad (0.1)$$

where f_{ref} is the reference frequency, f_c is the lower carrier, and n is the harmonic ratio of the two. This simple technique removes the geometrical doppler phase shift exactly; only the ionospheric contribution to the phase remains. It is decreased slightly by the harmonic ratio of the carriers, but that can be corrected by a f^{-1} correction to the reference phase. This allows a precise and accurate measurement of very small ionospheric phase perturbations, even at SHF where the geometrical doppler shift is large.

In the initial proposal for this work, we suggested a reference carrier near X-band, and two coherent measurement carriers at 4920 MHz and 1240 MHz. The utility of the dual measurement carriers is to make meaningful observations under all scintillation conditions. Even under conditions when the lower is strongly scattered, the second is still in weak scatter where all measurement assumptions are valid.

Additionally, we proposed an additional pair of carriers spaced closely to the 1240 MHz measurement line. This triplet of carriers can be used to measure the total electron content (TEC) of the ionosphere that is, by definition, coupled to the high-resolution structure data. The technique used is referred to as the second difference of phase ($\Delta_2\phi$) method. The phase differences of the three carriers can be computed as:

$$\Delta_2\phi = \phi(f_c + f_m) + \phi(f_c - f_m) - 2\phi(f_c) \tag{0.2}$$

where $\pm f_m$ are the carrier offsets about the center carrier f_c. By referring to the Equation 0.1, this provides a simple measurement of the ionospheric dispersion that is related to TEC as:

$$\Delta_2\phi = -2\kappa N_T \frac{f_m^2}{f_c^3} \tag{0.3}$$

The measurement becomes 2π ambiguous at some value of TEC, and this dictates the maximum triplet carrier spacing that is useful. On the other hand, the resolution of the measurement increases with separation.

The beacon spectrum was subsequently refined from that in the proposal. The original spectrum was based on exact harmonic frequency multiples for design simplicity of the beacon. That does, however, complicate receiver specifications, as well as limiting spacecraft antenna options. The proposed spectrum was also unnecessarily high in frequency, and early analysis indicated that carrier phase noise could limit ionospheric measurements under some conditions. The revised spectrum is lower in frequency, and consists of reference and measurement carriers that are not order-of-two harmonics. A quantitative look at the all-important phase noise issue has been made, and is reviewed below. This noise performance, and an estimate of the ionospheric conditions that TechSat21 would encounter, were used to derive the particular carrier frequencies. We have addressed three specific topics: (1) an optimum and practical frequency for the reference carrier, (2) an optimum choice for the lowest measurement carrier frequency and (3) the optimum frequency and triplet spacing for the TEC measurement.

Spectrum Design Considerations

Generation of the reference carrier (and the rest of the coherent beacon spectrum) starts from a relatively low (some tens to ~100 MHz) source oscillator. This frequency is multiplied up several (or many) times to provide the various phase coherent carriers in the spectrum and the reference carrier. Because the multiplication process also acts on the phase noise of the source oscillator, a very "clean" source oscillator is a necessity. It is the phase noise of the upper spectral carriers and the reference that will eventually limit the sensitivity and accuracy of the TecSat21 ionospheric measurement.

The TechSat21 beacon system would have used narrow bandwidth carriers, transmitted without modulation. Performance in such a system is dictated by what is referred to as the close-in phase noise of the measurement and reference carriers. These, in turn, are a function of the close-in phase noise of the source oscillator and the process used to multiply the source frequency to the transmitted carriers. Recent technology and techniques in source oscillator design have achieved amazingly low phase noise performance in off-the-shelf modules. Some examples of published phase noise specifications are shown in Table 1. The two source reference frequencies, 10 MHz and 100 MHz, represent the low and high range that we might use to multiply up for the transmitted carriers; additionally, most routine specifications are listed for these frequencies. The Oven Controlled (OCXO) units clearly have a performance advantage, but the Thermally Compensated (TCXO) units are better suited for spacecraft use. For TechSat21, that choice would have depended upon spacecraft power availability.

Table 1. Typical Source Module Performance

manufacturer and model	*carrier frequency*	*phase noise dBc/Hz at offset*				*note*
		10 Hz	*100 Hx*	*1,000 Hz*	*10,000 Hz*	
Valpey-Fisher VF1000	10 MHz	-110	-140	-150	-150	OCXO
Wenzel SpaceO-S/C	10 MHz	-125	-150	-165	----	OCXO
Wenzel ULNLF-S/C	10 MHz	-135	-160	-176	----	OCXO
Vectron TO-700	10 MHz	----	-110	-130	-135	TCXO
TCI HXO303	100 MHz	-80	-115	-145	-159	OCXO
Vectron CO-700	100 MHz	----	-130	-145	-157	OCXO
Wenzel ULNHF-S/C	100 MHz	----	-130	-160	-175	OCXO
Wenzel SpaceT-A/T	100 MHz	----	-120	-135	-160	TCXO
TCI XO835	100 MHz	-82	-105	-135	-160	TCXO

As has been noted, the source oscillator noise is increased by the harmonic multiplication to the measurement and reference frequencies. This depends somewhat on how the signals are multiplied, the choices being non-linear multiplication or phase-lock synthesis.

The original TechSat21 proposal considered a hardware configuration that used non-linear, active frequency multipliers. Frequency multipliers can be used in applications, such as ours, where the required bandwidth is much narrower than the input source frequency; otherwise, spurious and harmonic outputs become a problem. At frequencies close to the carrier, the input phase noise nominally multiplies as $20\log n$ where n is the

harmonic multiplication factor. The multiplier circuitry also adds a residual phase noise (typically f^{-1} device noise), although this noise is much lower than the multiplied source noise close to the carrier. The primary disadvantage of non-linear multipliers in a satellite application is their efficiency, since relatively high signal levels are required as inputs, and insertion losses are high.

More appropriate for satellite applications is the phase-lock oscillator (PLO) synthesis of higher frequency carriers. The PLO approach is more complex than non-linear multipliers, and direct analog PLO synthesis is impractical for small spacecraft designs. However, the demand for miniaturized telecommunications has produced a variety of high-performance "indirect" (i.e. mixed analog and digital) PLO devices and modules. The PLO synthesizer consists of a phase detector/filter, a voltage controlled oscillator (VCO) and an active feedback loop with a specified bandwidth. The VCO is configured to free run at the desired output frequency, and a digitally-divided replica is compared at the phase detector to the crystal source phase; when the divided- and source outputs fall within the loop bandwidth, the VCO is tuned to bring the two signals into phase lock. For spectral frequencies within loop bandwidth of the synthesizer, the output phase noise is a multiplied replica of the source oscillator noise. Like the non-linear multiplier, this is a $20\log n$ increase where n is the harmonic multiplication factor. Additionally, there are small noise contributions from the phase detector/divider circuit, and the operational amplifier in the active PLO loop. The digital noise from the phase detector/divider can be minimized by careful selection of the divider ratio, and the amplifier noise is negligible in a narrow-band application such as ours.

One of the early design questions was whether to use a lower or higher source oscillator in the satellite, the trade off being between inherent device performance and the need for a higher multiplication factor. Using data from Table I, the 10 MHz or 100 MHz source oscillators can be compared using the noise multiplication factor of 20 dB; in both cases, some additional small degradation (~2-3 dB) should be expected at the application frequency due to the phase lock divider electronics. The only model in Table I that spans both frequencies (Wenzel ULN series), and their 10 MHz OCXO, when multiplied up, would show superior phase noise performance over their 100 MHz unit. The difference is largest at close-in offsets, which is an important consideration. The low frequencies are important in the phase scintillation spectra that the system will measure. If this same advantage applies to TCXO units, it would suggest that we use a lower, rather than higher, source oscillator.

An end-to-end evaluation of how phase noise effects the ionospheric phase measurements includes both transmit and receive portions of the system. On the transmit side, the measurement carriers carry close-in phase noise, scaled up from the source oscillator. The receive side of the system is more complex. The reference carrier (with noise) is divided down to derive the local oscillators for the measurement carriers. This adds additional noise to the measurement, and that is what the scintillation data must compete with. These processes are described briefly in the following sections.

Reference Carrier

The reference carrier is the highest frequency line transmitted by the beacon. When received on the ground, that carrier is divided down to provide the phase references for the lower measurement carriers. Ideally, the reference should be free of (1) any ionospheric effects and, (2) phase noise. This is impossible to achieve, of course, but a practical compromise can be implemented.

The need to minimize ionospheric effects on the reference drives the frequency of the carrier upward, because of the inverse frequency dependence of dispersion effects. Any ionospheric dispersive phase in the reference will erode that of the measurement carriers, so the higher the frequency the better. In practice, however, the frequency must be only high enough that any scatter of the reference carrier remains weak. In this regime, a first-order inverse-frequency correction is highly accurate. In terms of phase variance, for example,

$$\sigma_m = \sigma_c \left(1 - n^{-2}\right) \tag{0.4}$$

where σ_m is the measured variance, σ_c is the corrected variance, and n is the harmonic ratio between the carrier and the reference. For a UHF measurement carrier and an S-band reference, this correction is about 7%.

The strongest scintillation in the natural ionosphere occurs in the equatorial anomaly region, and severe scattering is observed up through L-band frequencies. At S-band frequencies, however, the scatter is consistently weak; the only exceptions to this are on low-elevation paths that are not a primary TechSat21 concern. S-band or higher is therefore a logical choice as the coherent beacon reference carrier.

Minimizing the phase noise of the system is important, but it is less critical for reference carrier than it is for the measurement carriers. That is because when it is received, the signal is hard-limited and processed digitally (this will be described below). Obviously, the lower phase noise the better, but it has no particular bearing on the choice of a specific reference frequency.

One obvious requirement for the reference carrier is a high signal-to-noise ratio (SNR) at the ground receiver. This can be managed with adequate transmit power, a good quality high-gain receive antenna system, and proper RF design. Generally speaking, it is easier to obtain high SNR at 3 GHz than, for example, 10 GHz, if miniaturization and power efficiency on the satellite are a goal. For current design purposes, therefore, we have chosen 3 GHz as a nominal reference carrier frequency.

Lowest Measurement Carrier

The inverse frequency dependence of dispersive phase means that the lower the carrier frequency, the more sensitive the measurement of the ionosphere. Previous beacon

experiments[1], using older technology, have depended upon VHF carriers to obtain high-resolution dispersive phase measurements. VHF propagation measurements through the ionosphere suffer from a serious drawback, however. The measurements have been far from ideal in that non-dispersive antennas, compact enough for spacecraft use, are difficult (or impossible) to build. In the TechSat21 situation, the planar face could have been used for a high-performance VHF antenna, but is inconsistent with the primary space-based radar (SBR) mission function. A VHF patch array would have required an area as large as 5-7 m^2, and a VHF printed slot design would require more depth than is available. The smaller antennas required for UHF carriers are far more practical on spacecraft. At the higher frequency the antennas could be smaller, plus have their phase centers aligned with that of the reference carrier antenna, so the accuracy of the measurement is significantly improved.

With current hardware technology applied to both the beacon and receiver systems, it is possible to measure small changes in dispersive phase much more accurately than before. Our approach for the TechSat21 low carrier selection has been to estimate the end-to-end system phase noise as a function of carrier frequency. The frequency at which this exceeds our dispersive phase measurement goal is the upper limit for the lowest frequency carrier.

Phase noise accompanies the transmitted measurement carriers, and when they are received, additional noise is added. It is necessary to review how the system functions to estimate the receiver contribution to noise. It is assumed that the reference carrier is received with an assumed high SNR. It will be doppler-shifted is as much as ±100 kHz at the horizons, for an S-band carrier and the nominal TechSat21 orbit. The signal is amplified and divided down to create a "reconstructed source oscillator" signal. It is first applied to a GaAs MMIC frequency divider, which outputs a signal (with some small, fixed phase shift) at 1/4 the input frequency. This is a digital process in which the only quantity of interest is the phase of the signal; hence the lack of concern for the input phase noise of the reference carrier that was noted above. The MMIC divider does, however, contribute its own phase noise to the divided carrier, at the level indicated in Figure 2.

Under the current receiver design concept, the divided-by-four reference carrier is then mixed down to the same nominal frequency as the satellite source oscillator (but differing by geometrical and dispersive doppler shift). The mixer performance is critical, and the design is likely to be a high-level Termination Insensitive Mixer (TIM) to minimize spurious signals. The advantage of using a mixer is that it is inherently low noise: the phase noises of the input and mixing carriers simply add. The mixer carrier would be a premium OCXO (Wenzel ULN 100 MHz) with a phase noise spectrum shown in Figure 2. The published device specifications do not extend below 10 Hz, so noise in this regime is estimated as f^{-3} per the electronic character of the crystal oscillator.[2]

---

[1] Fremouw, E.J. et al, *Early results from the Wideband satellite experiment - Complex signal scintillation,* Rad. Sci., 13, number 1, January-February 1978.

[2] verbal communication, Charles Wenzel, Wenzel Associates, Inc., September 1999.

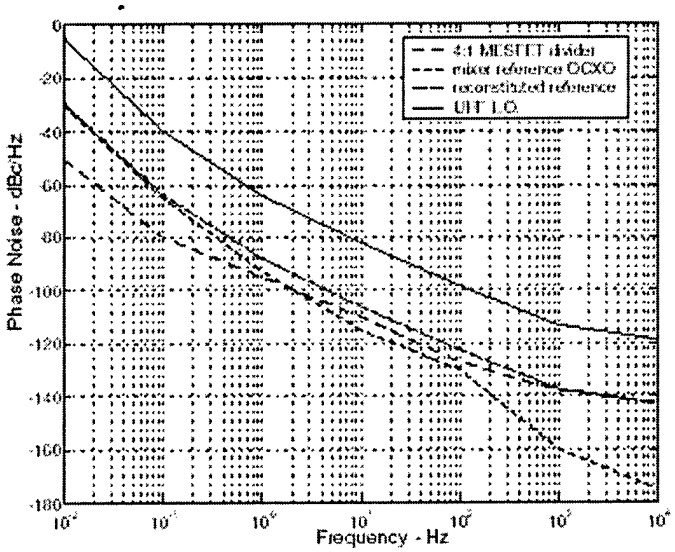

Figure 2. Estimated phase noise for the UHF measurement carrier.

An alternative receiver design would further divide the already-divided reference carrier using one of the emerging PCMOS (pico CMOS) divider devices. The devices are inherently noisy, but, when driving the measurement carrier PLO units, may have cumulative phase performance comparable to the mixer. This design option would have been pursued because its simplicity is an attractive option to implementing a TIM.

The mixed (or additionally divided) signal, as the reconstructed source oscillator, is phase locked, and used in PLO multipliers to derive the measurement carrier local oscillator (LO) signals. These mix the received measurement carriers to a lower intermediate frequency (IF) for additional processing and signal characterization. The phase noise of the receiver source oscillator, as has been noted, is the sum of the OCXO and GaAs divider phase noise. Like in the beacon transmitter, the close-in noise is multiplied in the LO output. In the case of a UHF carrier, that factor is an increase of ~24 dB, giving the final spectrum shown in Figure 2. This phase spectrum represents the system noise floor; if the spectrum of ionospheric dispersive phase changes fall below this floor, they cannot be quantified.

It is worthwhile to make a comparison between this measurement capability limit and the ionospheric spectrum that will be measured. Ionospheric irregularities are formed over a vast range of spatial scales, from global and tidal-scales (hundreds of kilometers) through convectively produced turbulent scales (meters). All of these scales appear in the dispersive phase of a transionospheric signal as the satellite (or the irregularities) move. At a receiver, the dispersive phase is measured in time, so the phase spectra are a function of frequency.

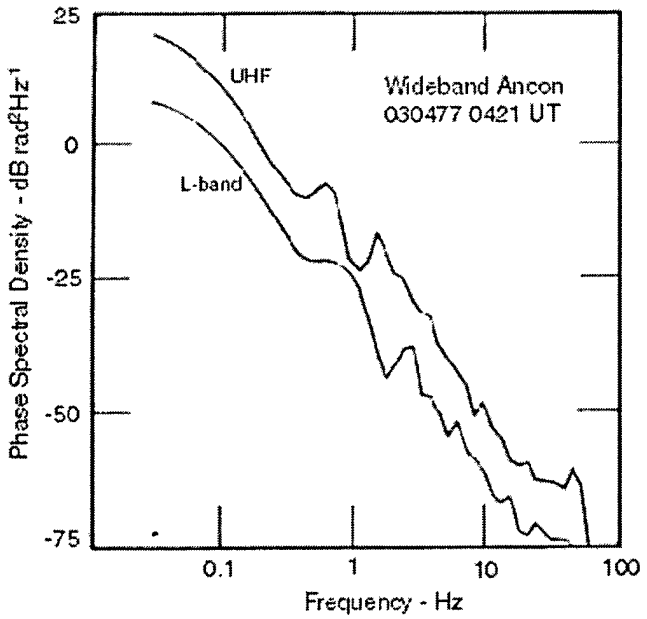

Figure 3. Typical phase spectrum at UHF and L-band at the equator.

A typical UHF phase spectrum measured at the equator is shown in Figure 3, and has a generally power-law form. The dominant "break scale" that can be discerned is typical of well-developed ionospheric turbulence. The largest scale irregularities of concern to the TechSat21 SBR are comparable to the integration aperture, perhaps tens of kilometers in size. The smallest of concern are tens of meters in size, some decades smaller, and more than 60 dB weaker. For a TechSat21-type orbit, a 35 km *in situ* spatial wavelength at F region altitudes corresponds to a temporal frequency of ~0.10 Hz at a beacon ground receiver; a 35 meter wavelength appears at ~100 Hz. The total measured change in dispersive phase represented in Figure 3 is many tens of radians.

The phase resolution that the system can achieve can be estimated by integrating the UHF LO phase noise spectrum in Figure 3 over the frequencies of interest. For our nominal ~800 MHz UHF measurement carrier, the 0.005 Hz through 1000 Hz portion of the noise spectrum integrates to a phase of less than 3°. In terms of ΔTEC this would reflect a change of less than 1×10^{13} electrons/m^2 along the propagation path. This is better than our nominal resolution goal, and confirms that there is no reason for a measurement carrier at lower than UHF frequencies.

TEC Carrier Triplet

Bulk ionospheric total content would have been routinely provided by GPS measurements during TechSat21 operations. By definition, however, GPS-derived TEC is large-scale, and cannot reproduce the short-term/small scale variations that will occur along the TechSat21 propagation paths. Furthermore, GPS measurements can include significant TEC contributions from the protonosphere and from ionospheric altitudes well above the TechSat21 orbit. In comparison, the second difference of phase ($\Delta_2\phi$) from a

phase-coherent carrier triplet provides an unambiguous TEC measurement that would be, by definition, coupled to the SBR and beacon transmission paths.

Selecting the triplet separation is a trade off between the resolution and the ambiguity of the measurement. Generally, the ambiguity in $\Delta_2\phi$ is less of a concern because of the GPS data; a few 2π wraps throughout an overpass, reconciled with the continuous dispersive phase, should be readily resolved with a vertical TEC value provided by GPS extrapolation.

The system phase noise in the receive process also has a bearing on choosing a triplet separation. This is a few dB higher than that UHF LO noise in Figure 2 because of the higher frequencies of the carriers. The noise spectra of the three carriers in the triplet are uncorrelated and thus add directly, so the $\Delta_2\phi$ is, inherently a "noisy" measurement. The triplet spacing should be large enough (i.e. high enough resolution) that small changes in TEC can be measured despite the noise.

Figure 4 shows the vertical TEC at what might be considered the minimum and maximum ionospheric configurations under which TechSat21 will operate. One is from mid-latitudes during the spring when TEC is minimal. The other is from Ascension Island in the equatorial anomaly region, measured during solar maximum. The units on the figure are TEC units, i.e. 10^{16} electrons/m^2. For an overhead TechSat21 overpass, the TEC observed at a 10° horizon is approximately 3 times larger than that at zenith (assuming a spherically stratified layer at F-region heights).

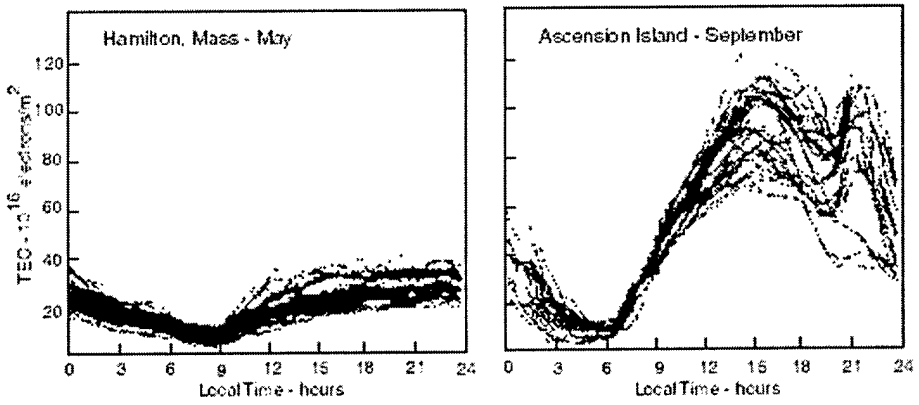

Figure 4. Range of TEC patterns that TechSat21 is likely to encounter.

We would argue that the carrier triplet separation should be selected to optimize the measurements for relatively low TEC conditions. This would account for the vast majority of conditions at all latitudes, and low TEC conditions are when GPS TEC measurements are most suspect, due to protonospheric and tropospheric contributions to signal phase. Furthermore, these are likely to be the conditions under which the TechSat21 SBR would undergo its initial performance evaluation. The penalty of low

TEC ambiguity would be that a measurement in the anomaly region would exhibit several 2π cycles during an overpass.

It is likely that the eventual $\Delta_2\phi$ resolution would have been limited by what kind of antenna is used for the triplet transmission. In particular, if a patch antenna were used, its bandwidth will be limited; this topic is discussed in more detail below. A different type of antenna (e.g. sinuous) would have the bandwidth, but may not be practical on TechSat21.

A triplet separation of about 100 MHz provides a good compromise between TEC resolution and antenna bandwidth requirements. For a ±100 MHz separation at 1240 MHz, $\Delta_2\phi$ becomes ambiguous at 7×10^{17} electrons/meter^2. For minimum TEC conditions, the measured $\Delta_2\phi$ at mid-latitudes would rarely become ambiguous. The minimum TEC at overhead under those same conditions ($\sim 5 \times 10^{16}$ electrons/meter^2) would be readily measured (0.44 radians).

In summary, our analysis suggests that the following frequency spectrum would work well for TechSat21:

3000 MHz	- coherent reference carrier
1140, 1240, 1340 MHz	- structure measurement and TEC
800 MHz	- weak structure measurement

These are approximate frequencies that would have been altered by frequency allocation availability, EMI and RFI issues with the radar or other spacecraft systems, had the system gone ahead.

Candidate Beacon Antenna Designs

The requirements for a beacon antenna suitable for TechSat21 are not trivial. In particular, the following issues need to be considered:

(1) *Circularity* -The beacon carriers (reference and measurement) all need to be transmitted using circular polarization; Faraday rotation effects make linear polarization unusable. Consistent axial ratios need to be maintained out to transmission angles approximately ±45° off boresite, i.e. the transmit geometry for routine ground data collections.
(2) *Coincident Phase Centers* - The phase centers of the antennas for the reference and measurement carriers need to be spatially coincident in order to obtain the most accurate ionospheric measurements.
(3) *Gain* - The beacon system efficiency and the ionospheric measurements would both greatly benefit if some transmit antenna pattern gain can be achieved. From space, a broad transmit beam is not necessary, and any increase in received signal SNR increases the measurement capability.

(4) *Dispersion* - A critical requirement for the TEC measurements is that the antenna used for the $\Delta_2\phi$ measurement is non-dispersive as a function of look angle. This has proven to be difficult in previous spacecraft, but that has been due to multipath scattering from an irregular spacecraft surface.

In the beacon design proposal, we briefly discussed multi-frequency antenna designs, such as helices or volutes that could satisfy the above requirements. However, those antennas are cylindrical and would have to extend a significant distance above a TechSat21 mounting plane. Early in the program, candidate spacecraft configurations made it clear that it would be difficult to integrate cylindrical antennas onto the spacecraft without seriously impacting SBR performance. Our emphasis has therefore been on antenna designs that are either planar, or close to it.

Patch Antennas

The popularity of patch antennas has grown enormously because of the telecommunications industry. They have also become common in radar arrays, both ground-based (such as wind profilers) and in space. In most cases, patch arrays are relatively simple to fabricate and can be made very lightweight. These attractions also apply to TechSat21, so much of our antenna review focussed on patch designs.

Patch antennas are not particularly small. A simple rectangular patch, placed over a thin dielectric slab, is nominally λ by $\lambda/2$ in size, where λ is the radio frequency wavelength in the dielectric. The resonant length is critical, making a patch antenna inherently narrowband. It is typically fed from the center of one long edge so that the horizontal electric field direction is the same at the other edge. Accordingly, the antenna radiates linearly, as if from two slots on the edges, with the maximum field strength upward from the patch surface.

The recent technology in patch antenna design has been driven by the need for smaller antennas, and preferably surface antennas, for cell telephones. Accordingly, the emphases have been on (1) reducing physical size and (2) broadening bandwidth. There has been some impressive innovation, and the practical state-of-the-art designs have advanced significantly.

Most of the patch antenna technology is reported either in *the IEEE Transactions on Antennas and Propagation* or the *IEE Proceedings, Microwaves, Antennas and Propagation.* More than 25 papers on patch antennas were published by these journals in 1998 or 1999, and provided the bulk of our technology review. Among these papers were ones that addressed a variety of topics appropriate to our design, such as arraying patches, dual-frequency patches and circular polarized solutions.

Our preliminary goal from the review was to ascertain that a straightforward patch antenna design could work for the beacon system. Very briefly, we are satisfied that basic patch elements can be built to provide the circularly polarized transmissions required from the beacon. Examples of practical approaches to this problem are

presented in Huang[3] and Huang et al.[4] Published data indicate that good polarization purity can be obtained from these and similar "cross slit" designs at boresite; generally speaking, this would imply adequate performance off boresite, although that is an issue that needs to be addressed. Further insight will be obtained from our mutual coupling modeling (see below), and the eventual fabrication of test antennas.

The pattern beamwidth of a single patch is much broader than the beacon transmit geometry requires. This suggests that an array of patches would be more appropriate, providing that the space is available. Arraying also neatly addresses the issue of coincident phase centers in that the arrays for the various carriers can be nested. A paper by Gentili and Salvador[5] illustrates that the arraying of a basic patch element can be effectively modeled and produces the expected overall pattern. The sharing of a single aperture by dual-frequency patch arrays was considered by Pokuls et al.[6]. Measured results show that sharing a single aperture does not adversely affect the patterns, i.e. that array interference is minimal in the main lobe patterns of the two arrays. It needs to be pointed out, however, that the mutual coupling problems are likely to be worse in the small array (four elements) that we propose. In the large array case, where the number of edge elements are small relative to the total, embedded pattern techniques can be used. This not the case with a small number of total elements. Darwood et al.[7] has developed a formal means to compensate for mutual coupling in a small array such as ours. We would have had to eventually go through a similar analysis and design adaptation.

The most difficult problem we faced using patch antennas for the beacon system was to obtain the bandwidth necessary for the triplet of carriers used to measure TEC. To minimize the space occupied by the beacon antennas, it is desirable that one array of patches is used to transmit all three carriers. As was previously indicated, a carrier triplet spaced approximately ±100 MHz about the central L-band line would provide good TEC data. This would require a bandwidth of about 16%, while typical patch antenna bandwidths are a few percent. For example; the circularly polarized design in the Huang[2] reference is about 4% bandwidth measured in terms of VSWR(<2:1), but only 2% bandwidth in polarization ratio (< 3 dB).

Bandwidth of a patch antenna can be increased in numerous ways. Parasitic oscillation posts are added, or multiple-frequency patches are stacked. Perhaps the most straightforward is to notch the basic patch, either singly or doubly. The notch(es) provide a reactive load near the center of the patch that is capacitive below, and inductive above the resonance frequency of the patch. This creates dual resonant frequencies above and

---

[3] Huang, C.Y., Designs for an aperture-coupled compact circularly polarised microstrip antenna, IEE Proc. - Microw. Antennas Propag., 146, No. 1, February 1999.

[4] Huang, C.Y., J.Y. Wu and K.L. Wong, Broadband circularly polarised square microstrip antenna using chip resistor loading, IEE Proc. - Microw. Antennas Propag., 146, No. 1, February 1999.

[5] Gentili, G.B. and C. Salvador, New serially fed polarisation-agile linear array of patches, IEE Proc. - Microw. Antennas Propag., 145, No. 5, October 1998.

[6] Pokuls, R., J. Uher and D.M. Pozar, Dual-frequency and dual-polarization microstrip antennas for SAR applications, IEEE Transactions on Antennas and Propagation, 46, No. 9, September 1998.

[7] Darwood, P., P.N. Fletcher and G.S. Hilton, Mutual coupling compensation in small planar array antennas, IEE Proc. - Microw. Antennas Propag., 145, No. 1, February 1998.

below that of the patch, and therefore increases bandwidth. Palit and Hamadi[8] provide a comparison between theory, model and measurement of notched patches. Their approach is successful, and they obtain bandwidths upwards of 35%.

Our concern with the broadband L-band patch is that even if the bandwidth can be obtained, the TEC measurement demands that it is circularly polarized and non-dispersive (in angle). Both these requirements add to the already-complex notched-patch design and may not even be feasible. The antennas for the other carriers can be proven using straightforward prototypes; the L-band unit will require significant modeling and empirical development.

If we assume for the time being that a suitable L-band patch can be developed, it is worthwhile to see how much space the total beacon patch array requires. As previously indicated, nesting of the separate patch array assures that their transmit phase centers are co-aligned. Although the specific beacon frequencies have not been defined, we have used the nominal spectrum (i.e. 800 MHz, 1240 MHz and the reference at 4800 MHz) to determine patch sizes and array spacing. One possible configuration, which is quite compact at 100-cm square, is shown in Figure 5.

The sizes of the patches shown are based on a cross-strip design that is aperture-coupled through a substrate dielectric. The aperture coupling approach (i.e. from a stripline-type feed below the ground-plane coupling slot) is attractive for TechSat21 application because it is adaptable to having MMIC devices installed adjacent to the antenna. For the illustration, the stripline feeds are shown (dotted) as they would be when driven by distributed amplifiers, and this makes the layout quite simple. When feeding the patches with single UHF and L-band sources, the stripline layout is more complex. However, each frequency uses a slightly different stripline feed substrate depth so multiple striplines can cross. In either case, the particular stripline layout must be included in the overall mutual coupling calculation that needs to be made.

The conclusion from our technical investigation of patch antennas is that, despite some attractions, the patch arrays have some practical disadvantages. First, to satisfy the need for coincident phase centers, the three arrays would take up a significant portion of the down-looking TechSat21 planar surface. Second, the stripline feed system for the patch system is relatively complex and would require considerable development and prototype time. The third (and most serious) problem is the uncertainty about the broad bandwidth performance of the L-band array used to measure TEC. Accordingly, we went on to consider alternative designs, and combinations of different antenna designs, that might be simpler, or better fit the TechSat21 spacecraft form and function.

[8] Palit, S.K., and A. Hamadi, Design and development of wideband and dual-band microstrip antennas, IEE Proc. - Microw. Antennas Propag., 146, No. 1, February 1999.

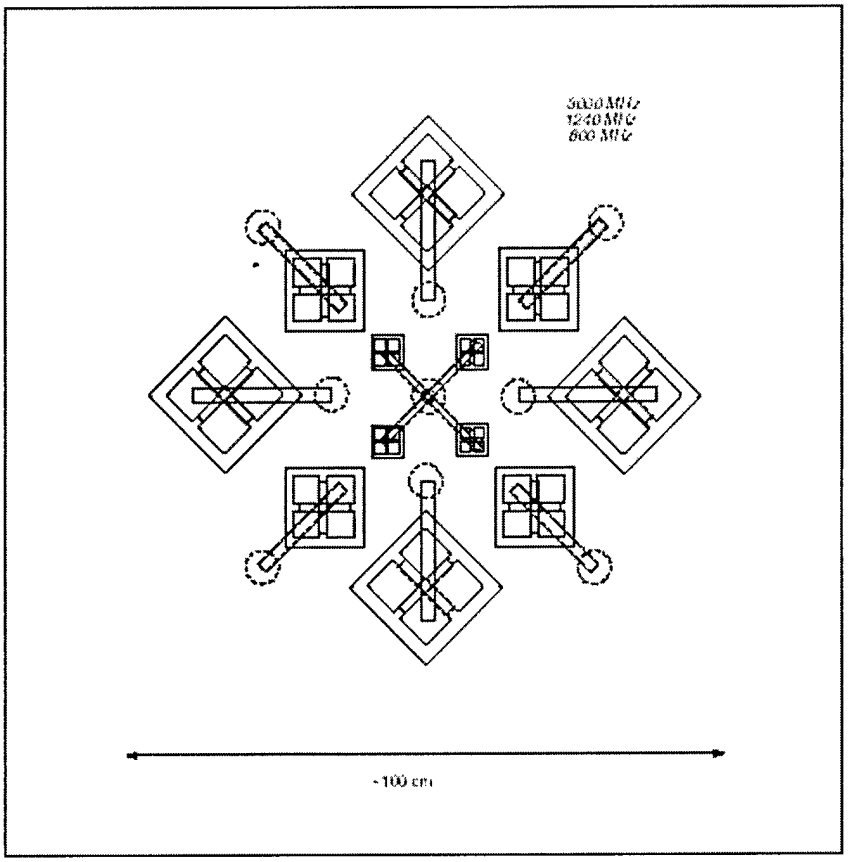

Figure 5. One candidate patch antenna layout for the beacon antennas showing striplines (dotted) and MMIC amplifier locations (dashed circles).

The nominal nested-patch arrays, with optimum dielectrics, would require an area about 18 in × 18 in. One of the antenna options that would require a smaller planar footprint smaller without sacrificing mission goals is the cavity-backed spiral antenna. However, in trade, it would require some depth behind the surface plane of the spacecraft.

The cavity-backed spiral is a "frequency independent" antenna which is fed with the combined beacon spectrum 800 MHz through 3000 MHz). As shown in Figure 6, its maximum diameter would be $\lambda/2$ at 800 MHz, or about 8 inches. The gain of the spiral is lower than the patch array design, but is adequate for the purposes of the experiment.

The primary unknown in this design is the exact depth necessary for the cavity to operate correctly at all frequencies from 800 MHz through 3000 MHz. The depth shown in Figure 6 (almost 4 inches) is scaled from similar, proven designs for a somewhat higher frequency range.

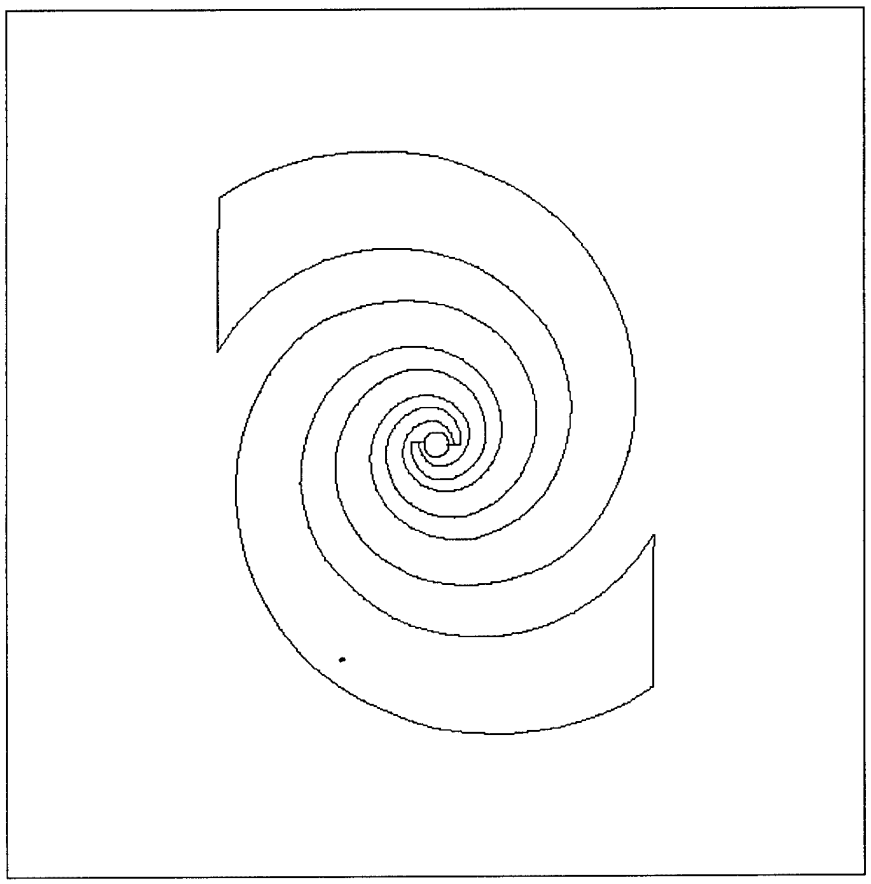

12in X 12 in square

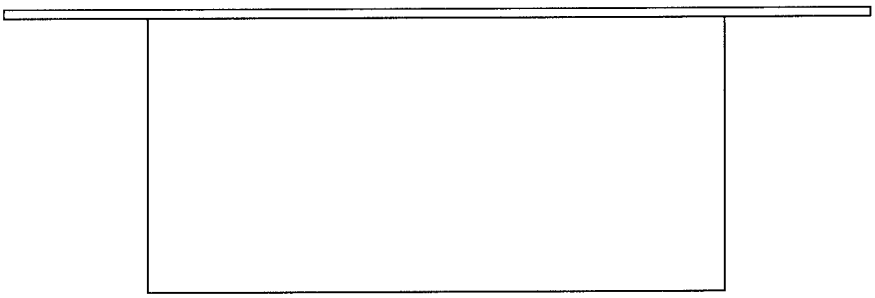

8.0 in diameter X 3.8 in deep cylinder

cavity-backed spiral: 0.50λ diameter, 0.25λ depth
- 800 MHz: 200 mm X 100 mm depth

Figure 6. Non-planar spiral antenna.

Almost Planar Annular Sector Radiating Line (ANSERLIN) Antenna

An antenna design that has been effectively used on high-speed aircraft is the annular sector, radiating-line (ANSERLIN) antenna[9]. It consists of an annular ring of conductor closely spaced above a ground plane, as illustrated in Figure 7. It is fed through "fins" between the ground plane and the surface, which makes it quite broad band (approximately 30%). This bandwidth capability means that the 800 MHz, 1140 MHz, 1240 MHz and 1340 MHz lines could share a single antenna. A second annular ring for 3000 MHz would be mounted at the center of the larger ring. The dimensions of the annular ring at 3000 MHz is about 50 mm, and for the 800 MHz-1340 MHz range, is about 140 mm. These dimensions are considerably smaller than the patch array. A particular attraction of this antenna is that it requires a depth of only about 20-mm at the lower frequency, or combined depth of about 35 mm for both antennas. This is approximately the same as the depth of a Supertile in the original TechSat21 SBR design.

By reputation, the ANSERLIN is relatively easy to design and to feed, although we have no experience with the design. The primary design question for TechSat21 is whether the two annular rings can be co-aligned without severe mutual coupling. Prior to cancellation of the beacon, the original developer of the ANSERLIN (Dr. Drewniak) was contacted for an informal discussion of this issue. He was confident that a straightforward dual-band ANSERLIN could be developed, and that the lower frequency element would provide the good dispersion qualities required for the TEC measurement. We had then agreed that a first step would be the use of EM modeling codes to model that antenna.

Hybrid Antenna - Non-planar Patch/Slot Array

If the beacon antenna assembly could extend a few inches behind the radiation plane, an 800 MHz slotted antenna can underlay the 3000 MHz and L-band patch arrays. This would reduce the size of the nested 1240 MHz and 3000 MHz patch arrays[10] to less than about 12 inches, as shown in Figure 8. The depth at which the slot ground plane would be mounted is approximately 3.75 in. It was suggested at review meetings that this assembly could take the place of one Supertile near a petal edge, although the mounting plane would have had to be adapted for the module depth.

The mechanical structure of this design would consist of double ground planes and multiple substrates to feed the patches and slots. Similar dual frequency designs have been successful in large spaceborne arrays.

---

[9] Drewniak, J.L., and P.E. Mayes, *IEEE Transactions on Antennas and Propagation*, Vol. 37, No. 3, March 1989.

[10] Huang, C.-Y., *IEE Proceedings -Microwave Antennas and Propagation*, Vol. 146, No. 1, February 1999.

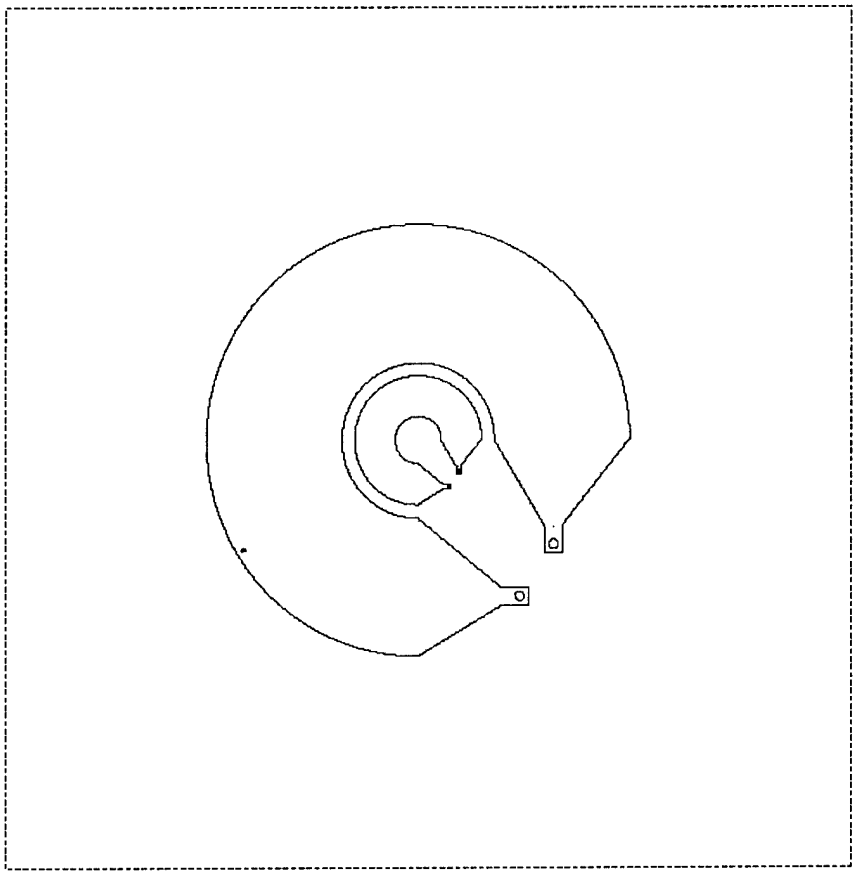

Figure 7. Almost planar annular sector, radiating line antenna.

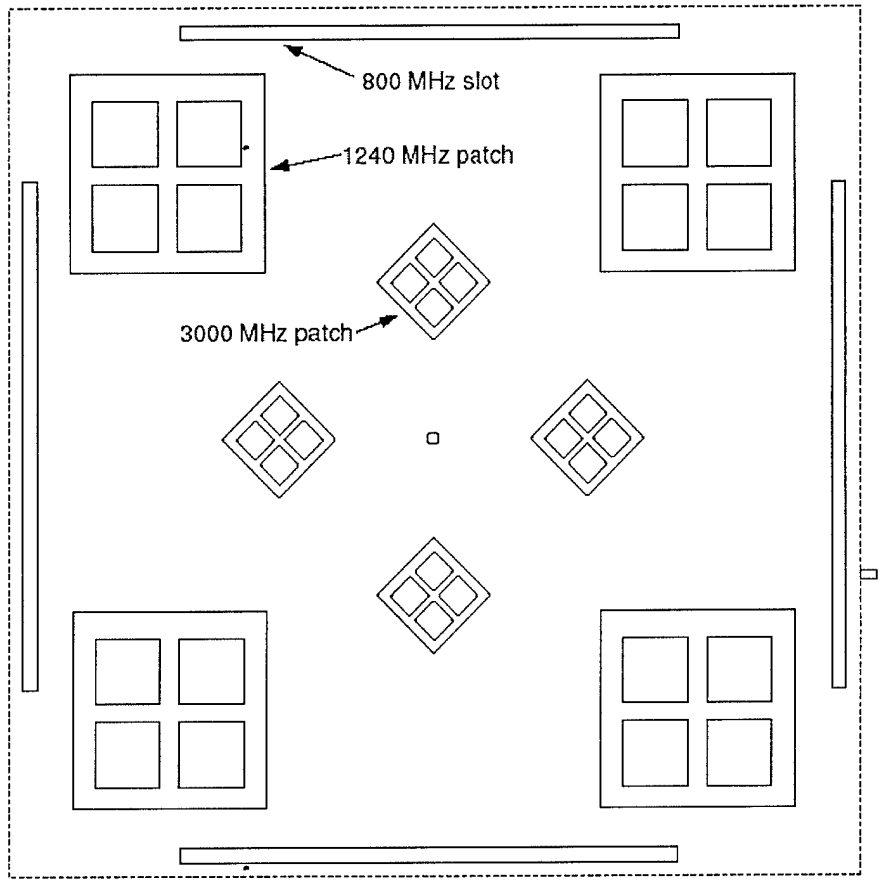

12 in X 12 in square

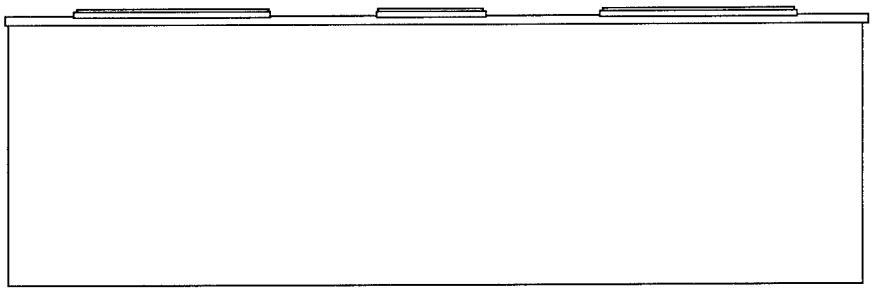

12 in X 12 in X 3.8 in cube

patches: 0.30λ square, 0.78λ separation
- 3000 MHz: 30 mm spaced 78 mm
- 1240 MHz: 73 mm spaced 188 mm

slots: 0.48λ length, 0.01λ width, 0.75λ separation,
0.25λ ground plane separation
- 800 MHz: 188 mm X 5 mm spaced 280 mm
93 mm ground plane depth

Figure 8. Small non-planar patch/slot array.

Hybrid Antenna - Planar Patch Array, 800 MHz Antenna Removed

One option is to reduce the original patch array size by removing the 800 MHz elements, i.e. discarding the 800 MHz line, or providing for an antenna elsewhere on the spacecraft. This would reduce the size of the nested 1240 MHz and 3000 MHz patch arrays to less than about 12 inches, as shown in Figure 9, and keep the assembly planar.

Relocating the 800 MHz antenna elsewhere sacrifices its coincident phase center with the 3000 MHz reference. This means that the precise removal of geometrical phase is somewhat compromised. However, the sensitivity to weak structure remains, and the ability to characterize the short-scale irregularities is unaffected. Processing of the 800 MHz would be more complex because it needs to be carefully reconciled with the 1240 MHz record to remove geometrical residuals.

Even separated from the patch assembly, the 800 MHz antenna installation is problematic. One option is to place orthogonal $\lambda/2$ elements along the edges of one petal. The effective pattern of this configuration has not been determined, but will be complex. The effective patterns need to be estimated, but may not be usable.

Distributed Antenna Elements

If no space could be made available on the SBR petal surface, an option would be to distribute the antenna elements around the bottom of the spacecraft body. There are four small areas that overlap the central petal, and rough estimates based on petal size and barrel dimensions (Figure 10) show the available "gusset" space to be about 8 in^2. This is too small for the patch elements, but printed slots could be used at 3000 MHz and 1240 MHz per the sketch.

Preliminary pattern calculations suggest that coincident phase centers cannot be achieved using the gusset areas. At such a wide spacing, arraying the S-band and L-band elements will generate grating lobes in the patterns and make any dispersive phase measurements virtually impossible.

The alternative would be to use the gusset areas to mount individual antennas for the S-band, and three L-band frequencies. In principal, the spacecraft attitude would be known with some precision, and the phase center offsets could be compensated for in processing. Modeling of the array would indicate how accurately the dispersive phase could be calculated, but it should be adequate for SBR operation diagnostic purposes.

The 800 MHz antennas would have to be dropped, or mounted elsewhere. If the gusset size could be extended to accommodate the approximately 8-inch diameter of the ANSERLIN antenna, a variety of design options become available.

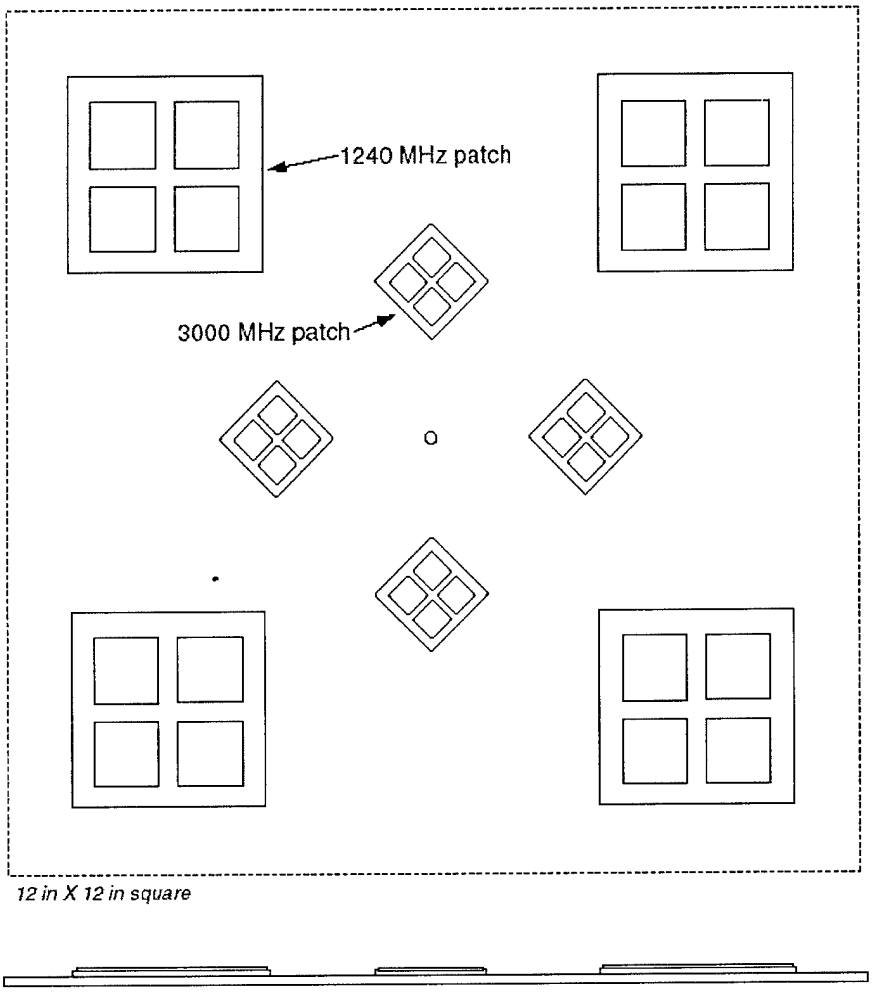

patches: 0.30λ square, 0.78λ separation
- 3000 MHz: 30 mm spaced 78 mm
- 1240 MHz: 73 mm spaced 188 mm

Figure 9. Small planar patch array, 800 MHz antenna elsewhere.

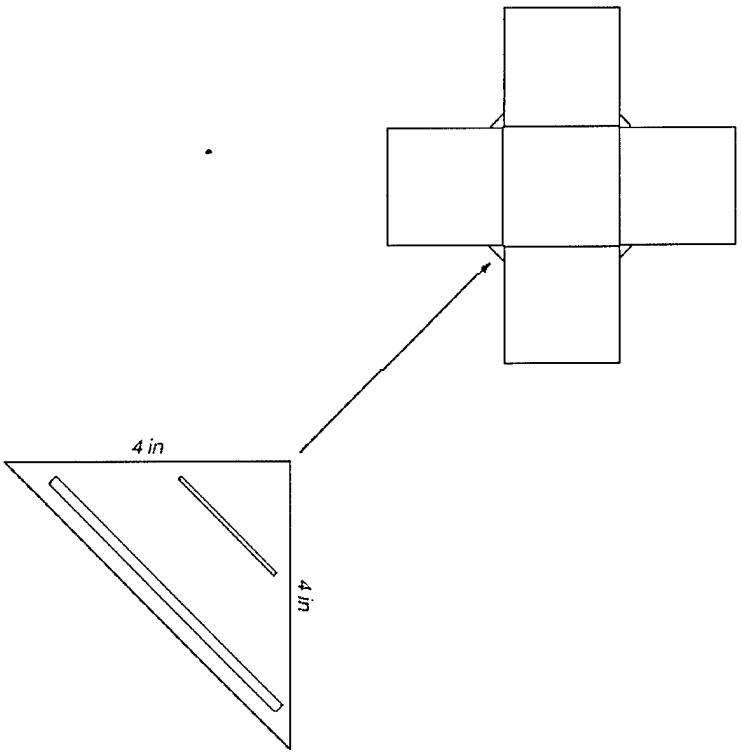

slots: 0.48λ length, 0.01λ width
0.25λ ground plane separation

- 3000 MHz: 48 mm X 1 mm
  25 mm ground plane depth
- 1240 MHz: 116 mm X 2.5 mm
  60 mm ground plane depth

Figure 10. Distributed antenna elements.

Alternative Antenna Mounting

The primary alternatives for mounting a variety of beacon antenna designs were (1) to replace a single radar super tile with the beacon antenna assembly, or (2) to distribute the antenna elements around the edges or gussets of the radar panels. Additionally, it was suggested that an additional design (3) would be to add a secondary fold out panel to carry orthogonal element pairs for each of the beacon carriers.

As pointed out above, the distributed design would be acceptable only if the science goals of the beacon experiment were to be sacrificed. More specifically, the science observations require coincident phase centers, and that cannot be achieved with widely distributed elements; severe grating lobes dominate the pattern, even if the beam is spoiled. If the science goals are dropped, the antenna assemblies could be separated, with different frequencies residing in different gussets. This arrangement is unattractive mechanically, in that three separate antenna assemblies must be developed.

The third option is an adaptation of the early suggestion that the beacon antenna be mounted on a separate panel. As with the early design, the beacon panel would fold out from one of the radar panels, although, dual orthogonal patch elements would be used at each frequency to minimize the size of the panel, and make it triangular in shape. The primary problem with the design is that the fold out would have to be nearly planar. In the configuration proposed (printed elements on a plane), the antenna patterns are influenced primarily by the spacecraft body surface, and are skewed to the side rather than downward. Good performance could be obtained if the assembly could have enough depth to accommodate a ground plane spaced at about $\lambda/4$ (a few inches) from the element plane.

With none of these alternatives being attractive, we suggested yet another adaptation of the separate panel idea. The difference was that this would be a small panel that folds out from the side of the spacecraft body. In our opinion, this had several advantages over a panel mounted to the radar assembly:

1) it provided independence between the beacon and radar system designs. The radar design could be altered (e.g. to use more, fewer, or different shaped panels) without impact on the beacon antenna.
2) it was compact enough that it has little dependence on the size or shape of the spacecraft body (e.g. shorter length, smaller diameter, fewer floors).
3) it integrated the entire beacon function into the spacecraft body to simplify power and RF feeds.
4) it was mechanically simple, particularly if a coaxial feed system were used.
5) it simplified integration testing of the beacon.
6) it satisfied all the engineering and science goals originally proposed for the beacon system.

The size of the fold out panel depends upon the choice of an antenna design, although we strongly suggested the annular ring (ANSERLIN) design. This design required the minimal space, the antenna, per se, being about 140 mm (5.5 in) in diameter. The ANSERLIN is not completely planar, but requires only about 30 mm (1.4 in) to accommodate the two antenna planes and their feed assemblies. Figure 11 is a sketch of the ANSERLIN antenna of these dimensions, as it would look prior to deployment from the spacecraft body. The figure also shows the antenna disc attached to an arm that hinges from the spacecraft body to hold the antenna clear of the panel gussets. Figure 12 shows the antenna and its mounting assembly deployed on an arm that is about 16 inches long. Because the ANSERLIN antenna can be coaxially fed, a simple reformable cable assembly would have provided the flexibility required for deployment.

Beacon-Based Precise Position Determination System

A major issue for the TechSat21 satellite cluster was the need to constantly know where each member is relative to the others. In close formation, collisions between spacecraft were an issue. In normal or wide formation, precision relative position information is essential to proper SBR performance. The coherent beacon design lends itself to a straightforward ranging method. The same method used to provide phase coherence among multiple radio beacons in the cluster could be readily applied to precise position determination. The method is relatively easy to implement, requires minimal resources, and has ancillary benefits for system operation and maintenance.

The technique uses a series of low-power UHF signals exchanged among the members of the cluster. More specifically, each satellite transmits a narrow triplet of coherent CW carriers that are received by the other satellites. The phases of the individual carriers in the triplet are many times 2π ambiguous between the transmitter and receiver. However, the specific frequencies in any triplet are chosen such that their collective phase differences are unambiguous over ranges out to several kilometers. The resolution of the measurement is limited by the accuracy of the phase measurement -- approximately 1° at UHF, or about 1 mm.

Implementation of the transmitter and receive hardware (call the combination the "sensor") is straightforward. As shown in Figure 13, two small antennas are required, one for transmit and one for receive; these need not be efficient, and small stubs will suffice. The transmitter makes use of the ultra-stable beacon frequency reference to drive the phase-locked oscillators used for the triplet generation. On the receive end, the beacon reference is again used to mix and digitally down-convert the triplet signals. In practice, the analog hardware is somewhat more complex than in the figure, but is of standard design. The digital IQ data from the digital down-converter can be readily processed in a microcontroller, and the phase values sent off to the telemetry buffer. All components can be miniaturized, and require very little power and space.

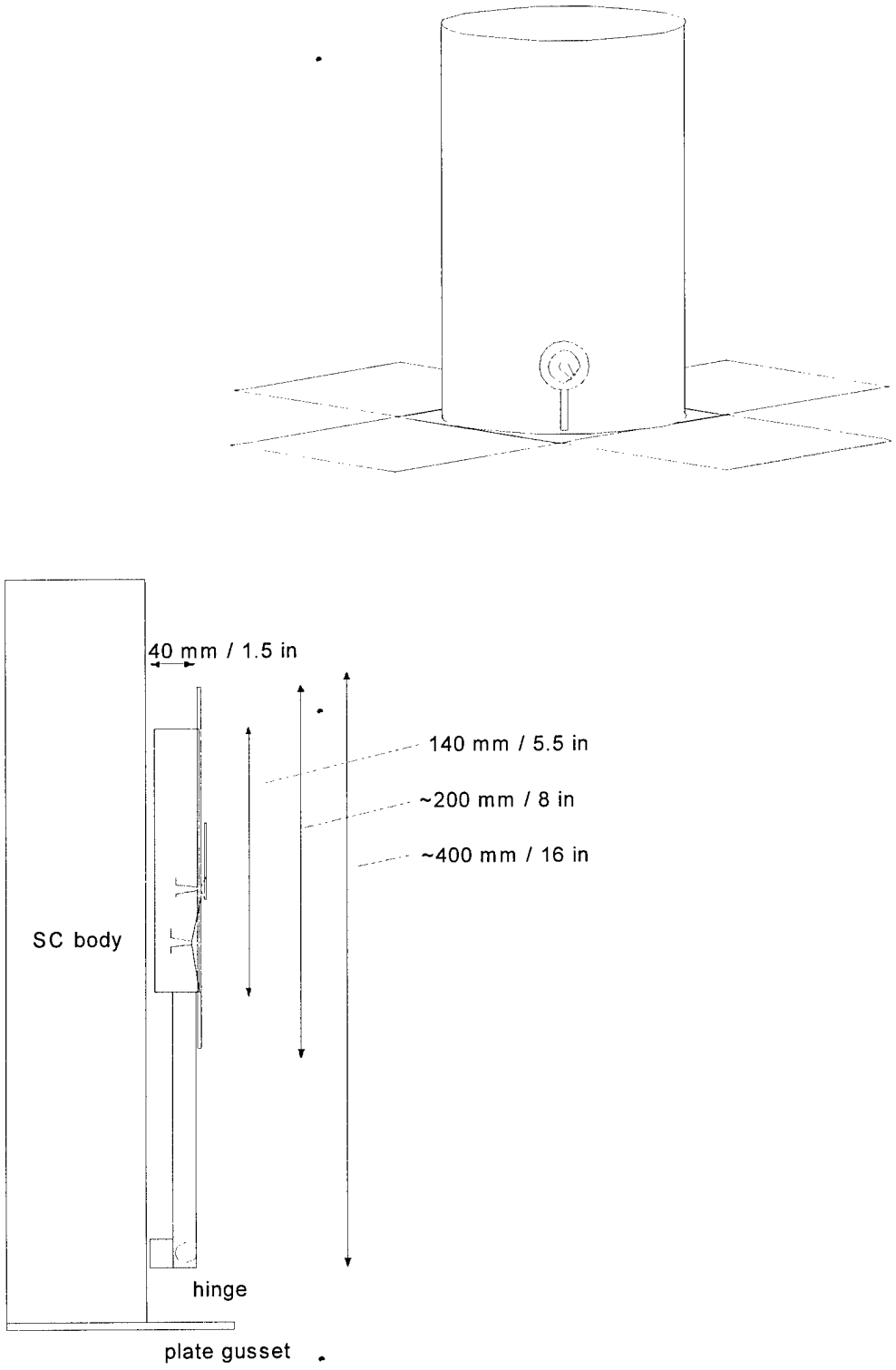

Figure 11. Body-mounted beacon antenna in stowed position.

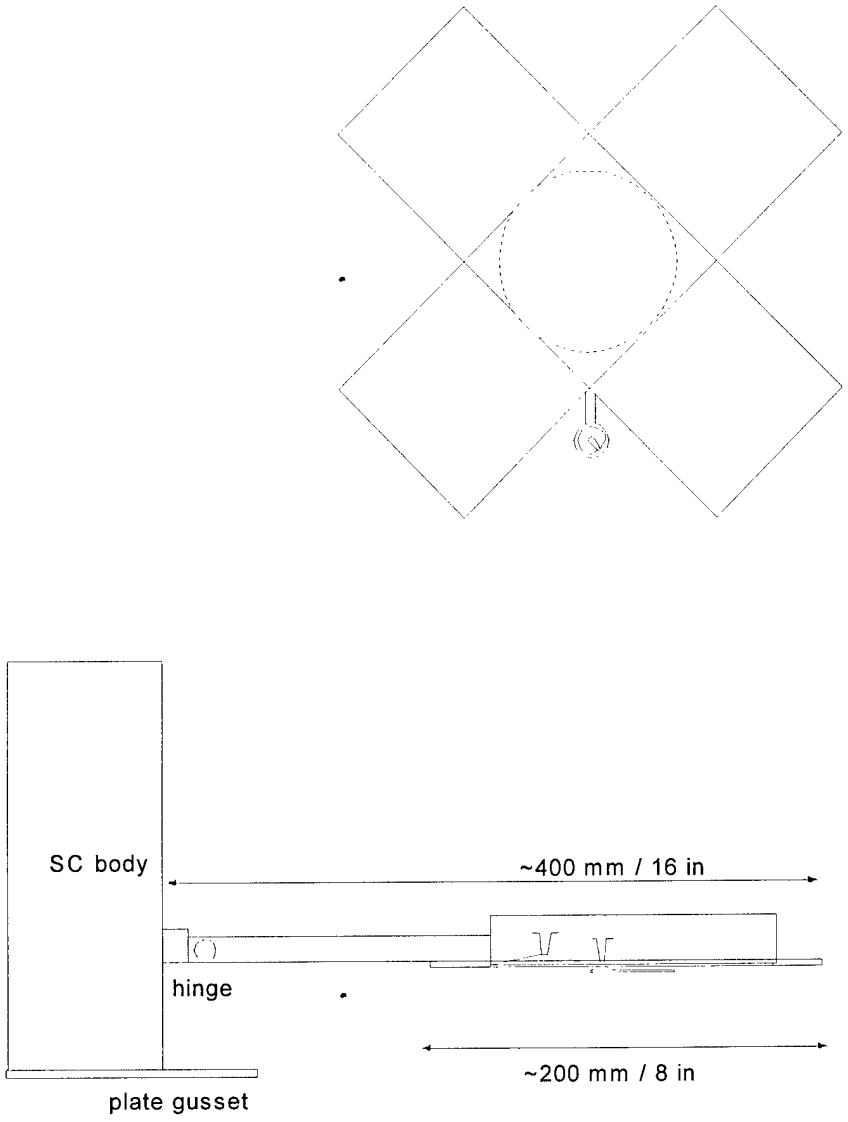

Figure 12. Body-mounted beacon antenna after release.

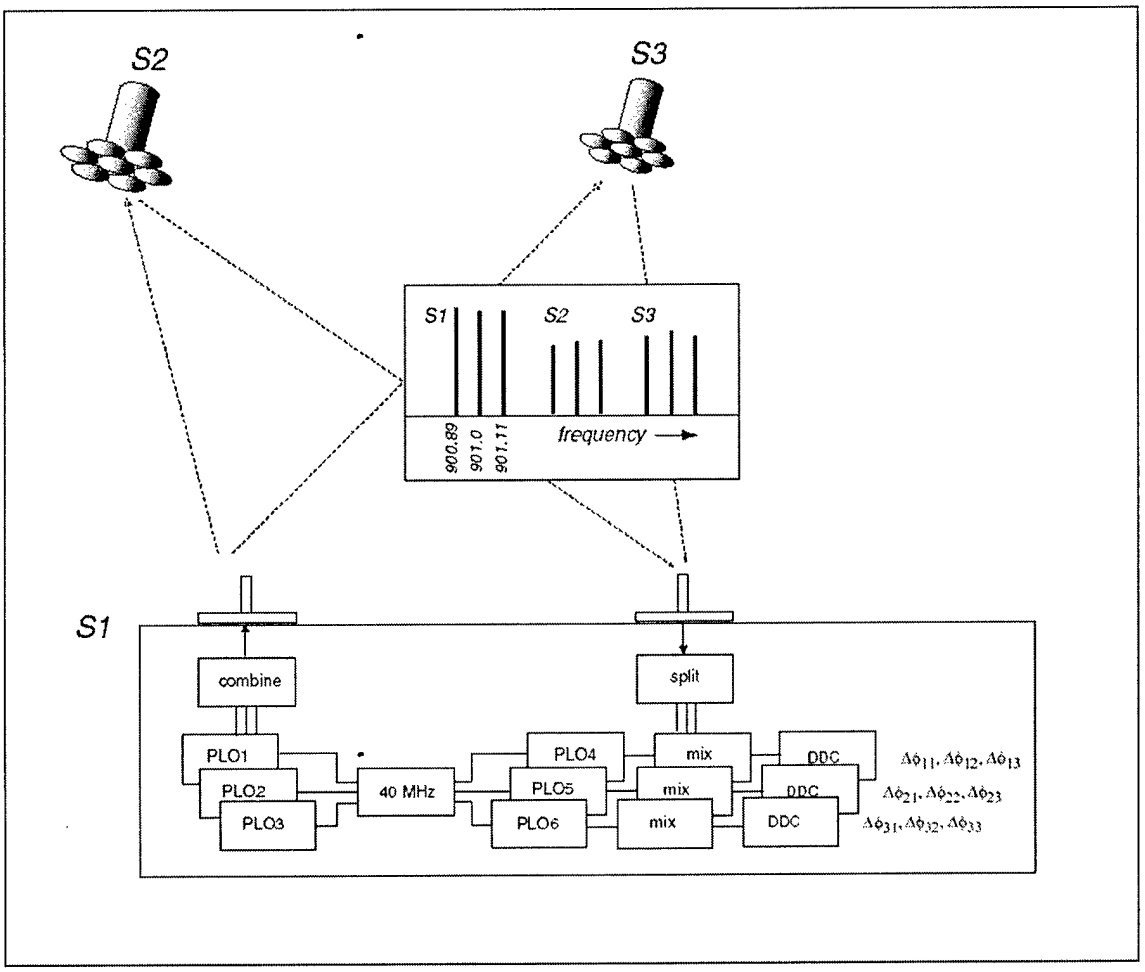

Figure 13. Ranging scheme using one sensor per satellite.

A good frequency band for the ranging carriers is 800-900 MHz. This provides a short enough wavelength for good resolution, and many ASIC components are available (should a prototype be built). The separation of the carriers within the triplets is a practical choice; if they are too closely spaced, separation of the triplet in the hardware is more difficult. The example below provides a sample spectrum that works well, but is, by no means, unique.

A single sensor on each satellite of the nominal three-member cluster would provide six independent ranges, which is not enough for satellite position determination. Two sensors per satellite, installed at either end of the spacecraft body (separated by ~7 meters), would solve this problem. It would provide a total of 24 inter-satellite paths, enough to be inverted into satellite positions.

A simple model has been developed to illustrate the technique using two sensors per satellite, and is attached as Appendix A. The program takes the relative satellite positions

as inputs, and calculates the exact ranges and the corresponding modulo 2π phases for each triplet. These are then processed to extract range simply by seeing at what 2π multiple the three phase values best match those "measured". The collective ranges are then used in a non-linear least-squares derivation of satellite position. Note that the satellites are always nadir pointing in the model, but the processing is entirely general (out to ranges of a few kilometers).

The results in Tables 2 and 3 are from the model, both collinear and triangular clusters; the processing of these "ideal" data is consistent to several decimal places. In reality, there will be small phase errors in the measurement, thermal changes in the spacecraft dimensions, and a number of other effects. If there had been interest in the technique, the effects of random and systematic phase errors and spacecraft size changes can be added to the model, and could be analyzed in some detail. One advantage of the least-squares approach for the position solution (as used in the example code) is that if those errors are small, they will be compensated for to some degree. An additional advantage is that range information from other onboard sensors (GPS and ISL) can be added into the solution to further improve the statistical accuracy of the position estimate.

One practical concern is exactly where the short stub antennas could be mounted on the spacecraft. The top is not an issue, but the bottom, per se, would have been in the radar field of view. An attractive site would be the side of a petal, although this could be shielded from the other satellites as the satellite rotates. This would suggest that a third sensor be added for ranging from the opposite petal. Statistically, the use of three ranging points per satellite is very powerful, and would additionally improve the accuracy of any position estimation.

It should also be noted that, in addition to range, the technique provides continuous range-rate information for each inter-satellite path. It seems like these data would be invaluable, both operationally and in detailed system analysis. For example, a collision-avoidance system could use this information in its on-board algorithms. On the ground, the data would be ideal for modeling of the cluster dynamics, and prediction of its behavior during reconfiguration. Derivation of spacecraft attitude, which is critical for geolocation among other things, would be considerably simplified.

Table 2

Example Output 1, Collinear Stub Placement

SPECIFIED POSITION:

	X	Y	Z
SAT 1	-210.000000	0.000000	2.000000
SAT 2	-5.000000	0.000000	0.000000
SAT 3	200.000000	1.000000	0.000000

EXACT RANGES:

	top1	bot1	top2	bot2	top3	bot3
top1	0.000000	7.000000	205.009756	205.197466	410.006098	410.099988
bot1	7.000000	0.000000	205.060967	205.009756	410.031706	410.006098
top2	205.009756	205.060967	0.000000	7.000000	205.002439	205.121915
bot2	205.197466	205.009756	7.000000	0.000000	205.121915	205.002439
top3	410.006098	410.031706	205.002439	205.121915	0.000000	7.000000
bot3	410.099988	410.006098	205.121915	205.002439	7.000000	0.000000

PHASE-DERIVED RANGES:

	top1	bot1	top2	bot2	top3	bot3
top1	0.000000	0.000000	205.009756	205.197466	410.006098	410.099988
bot1	0.000000	0.000000	205.060967	205.009756	410.031706	410.006098
top2	205.009756	205.060967	0.000000	0.000000	205.002439	205.121915
bot2	205.197466	205.009756	0.000000	0.000000	205.121915	205.002439
top3	410.006098	410.031706	205.002439	205.121915	0.000000	0.000000
bot3	410.099988	410.006098	205.121915	205.002439	0.000000	0.000000

NLLS-DERIVED POSITION:

	X	Y	Z
SAT 1	-37.371419	66.386334	137.369121
SAT 2	166.124444	91.174109	135.369121
SAT 3	369.499391	116.954548	135.369121

NLLS-DERIVED RANGES:

	top1	bot1	top2	bot2	top3	bot3
top1	0.000000	7.000000	205.009756	205.197466	410.006098	410.099988
bot1	7.000000	0.000000	205.060967	205.009756	410.031706	410.006098
top2	205.009756	205.060967	0.000000	7.000000	205.002439	205.121915
bot2	205.197466	205.009756	7.000000	0.000000	205.121915	205.002439
top3	410.006098	410.031706	205.002439	205.121915	0.000000	7.000000
bot3	410.099988	410.006098	205.121915	205.002439	7.000000	0.000000

Table 3

Example Output 2, ~Triangular Stub Placement

```
SPECIFIED POSITION:
            X           Y           Z
 SAT 1-2000.000000 1000.000000    0.000000
 SAT 2    0.000000    0.000000    0.000000
 SAT 3 2000.000000 1000.000000    2.000000

 EXACT RANGES:
          top1        bot1        top2        bot2        top3        bot3
 top1    0.000000    7.000000 2236.067977 2236.078934 4000.000500 4000.003125
 bot1    7.000000    0.000000 2236.078934 2236.067977 4000.010125 4000.000500
 top2 2236.067977 2236.078934    0.000000    7.000000 2236.068872 2236.073568
 bot2 2236.078934 2236.067977    7.000000    0.000000 2236.086090 2236.068872
 top3 4000.000500 4000.010125 2236.068872 2236.086090    0.000000    7.000000
 bot3 4000.003125 4000.000500 2236.073568 2236.068872    7.000000    0.000000

 PHASE-DERIVED RANGES:
          top1        bot1        top2        bot2        top3        bot3
 top1    0.000000    0.000000 2236.067977 2236.078934 4000.000500 4000.003125
 bot1    0.000000    0.000000 2236.078934 2236.067977 4000.010125 4000.000500
 top2 2236.067977 2236.078934    0.000000    0.000000 2236.068872 2236.073568
 bot2 2236.078934 2236.067977    0.000000    0.000000 2236.086090 2236.068872
 top3 4000.000500 4000.010125 2236.068872 2236.086090    0.000000    0.000000
 bot3 4000.003125 4000.000500 2236.073568 2236.068872    0.000000    0.000000

 NLLS-DERIVED POSITION:
            X           Y           Z
 SAT 1 1514.131175-1940.028262  378.116298
 SAT 2  384.645656  -10.193434  378.116298
 SAT 3 1250.822208 2051.295877  380.116298

 NLLS-DERIVED RANGES:
          top1        bot1        top2        bot2        top3        bot3
 top1    0.000000    7.000000 2236.067977 2236.078934 4000.000500 4000.003125
 bot1    7.000000    0.000000 2236.078934 2236.067977 4000.010125 4000.000500
 top2 2236.067977 2236.078934    0.000000    7.000000 2236.068872 2236.073568
 bot2 2236.078934 2236.067977    7.000000    0.000000 2236.086090 2236.068872
 top3 4000.000500 4000.010125 2236.068872 2236.086090    0.000000    7.000000
 bot3 4000.003125 4000.000500 2236.073568 2236.068872    7.000000    0.000000
```

Appendix A. Ranging Triplet Model

```
************************************************************************
*  model of the triplet ranging technique for TechSat21
*   - Bob Livingston, Scion Associates 2/2000
************************************************************************
      IMPLICIT REAL*8 (A-H,O-Z)

      common/drcos/range(6,6)
      external fcn_pos

      dimension frequency(6,3), wavelength(6,3)
      dimension position(6,3), center(3,3), pivot(9)
      dimension phase(3), phasemod(3)
      dimension phasetest(3), phasetestmod(3)
      dimension phasefit(3), path(6,6), fitrange(6,6)
      dimension fvec(24), wa(600), iwa(60)

      data tpi/6.2831853/
      data frequency/900.89,  901.0,  901.11,
     .               901.99,  902.1,  902.21,
     .               903.09,  903.2,  903.31,
     .               904.19,  904.3,  904.41,
     .               905.29,  905.4,  905.51,
     .               906.39,  906.5,  906.61/

      write(6,1)
      read(5,*) center(1,1), center(1,2), center(1,3)
      write(6,2)
      read(5,*) center(2,1), center(2,2), center(3,3)
      write(6,3)
      read(5,*) center(3,1), center(3,2), center(3,3)

      do 1001 i = 1,6
      do 1001 j = 1,3
      wavelength(i,j) = 300./frequency(i,j)
 1001 continue

*******************************
* antenna offsets from centers
*******************************
      position(1,1) = center(1,1) + 0.
      position(2,1) = center(1,1) + 0.
      position(3,1) = center(2,1) + 0.
      position(4,1) = center(2,1) + 0.
      position(5,1) = center(3,1) + 0.
      position(6,1) = center(3,1) + 0.

      position(1,2) = center(1,2) + 0.
      position(2,2) = center(1,2) + 0.
      position(3,2) = center(2,2) + 0.
      position(4,2) = center(2,2) + 0.
      position(5,2) = center(3,2) + 0.
      position(6,2) = center(3,2) + 0.

      position(1,3) = center(1,3) + 3.5
      position(2,3) = center(1,3) - 3.5
      position(3,3) = center(2,3) + 3.5
      position(4,3) = center(2,3) - 3.5
      position(5,3) = center(3,3) + 3.5
      position(6,3) = center(3,3) - 3.5

      open(unit=16,file='ts21.dat',status='unknown')
      close(unit=16,status='delete')
      open(unit=16,file='ts21.dat',status='new')
```

```
*********************
* exact path ranges
*********************
      do 1005 i = 1,6
      distance = 0.
      rangefit = 0.
      do 1004 j = 1,6
      distance = dsqrt( (position(j,1)-position(i,1))**2 +
     .                  (position(j,2)-position(i,2))**2 +
     .                  (position(j,3)-position(i,3))**2 )
      path(i,j) = distance

      rangefit = 0.
      range(i,j) = rangefit

*********************
* phases, this path
*********************
      do 1003 k = 1,3
      phase(k) = tpi * distance/wavelength(i,k)
      phasemod(k) = dmod(phase(k), tpi)
 1003 continue
      if( distance .le. 10) goto 1004

*********************************************************
* search for phase difference combination (out to 5000 m)
*********************************************************
      bestfit = 1.e6
      do 1010 k = 1,15000
      phasepath = tpi*k + phasemod(2)
      rangetrial = phasepath * wavelength(i,2)/tpi
      fit = 0.
      do 1011 l = 1,3
      phasetest(l) = tpi*rangetrial/wavelength(i,l)
      phasetestmod(l) = dmod(phasetest(l), tpi)
      phasefit(l) = phasemod(l)-phasetestmod(l)
      fit = fit + sqrt(phasefit(l)**2)
 1011 continue
      if( fit .ge. bestfit) goto 1012
      bestfit = fit
      rangefit = rangetrial
 1012 continue
 1010 continue
      range(i,j) = rangefit
 1004 continue
 1005 continue

************************************
* initialize non-linear least-squares
************************************
     lwa = 600
      m = 24
      n = 9
      tol=1.d-6

      do 1101 i = 1, 3
      pivot(i  ) = 1.d0
      pivot(i+3) =   1.d0
      pivot(i+6) =   1.d0
 1101 continue

****************************************
* non-linear least-squares from Argonne
****************************************
      call lmdif1(fcn_pos, m ,n , pivot, fvec, tol,
     1            info, iwa, wa, lwa)
       write(6,*) info

**********************
* verification ranges
```

```
**********************
      position(1,1) = pivot(1)
      position(2,1) = pivot(1)
      position(3,1) = pivot(4)
      position(4,1) = pivot(4)
      position(5,1) = pivot(7)
      position(6,1) = pivot(7)

      position(1,2) = pivot(2)
      position(2,2) = pivot(2)
      position(3,2) = pivot(5)
      position(4,2) = pivot(5)
      position(5,2) = pivot(8)
      position(6,2) = pivot(8)

      position(1,3) = pivot(3) + 3.5
      position(2,3) = pivot(3) - 3.5
      position(3,3) = pivot(6) + 3.5
      position(4,3) = pivot(6) - 3.5
      position(5,3) = pivot(9) + 3.5
      position(6,3) = pivot(9) - 3.5

      do 1105 i = 1,6
      distance = 0.
      rangefit = 0.
      do 1104 j = 1,6
      distance = dsqrt( (position(j,1)-position(i,1))**2 +
     .                  (position(j,2)-position(i,2))**2 +
     .                  (position(j,3)-position(i,3))**2 )
      fitrange(i,j) = distance
 1104 continue
 1105 continue

***************
* output print
***************
      write(16,4)
      write(16,5) center(1,1), center(1,2), center(1,3)
      write(16,6) center(2,1), center(2,2), center(2,3)
      write(16,7) center(3,1), center(3,2), center(3,3)
      write(16,8)
      write(16,9)  (path(1,k), k=1,6)
      write(16,10) (path(2,k), k=1,6)
      write(16,11) (path(3,k), k=1,6)
      write(16,12) (path(4,k), k=1,6)
      write(16,13) (path(5,k), k=1,6)
      write(16,14) (path(6,k), k=1,6)
      write(16,15)
      write(16,9)  (range(1,k), k=1,6)
      write(16,10) (range(2,k), k=1,6)
      write(16,11) (range(3,k), k=1,6)
      write(16,12) (range(4,k), k=1,6)
      write(16,13) (range(5,k), k=1,6)
      write(16,14) (range(6,k), k=1,6)
      write(16,16)
      write(16,5) pivot(1), pivot(2), pivot(3)
      write(16,6) pivot(4), pivot(5), pivot(6)
      write(16,7) pivot(7), pivot(8), pivot(9)
      write(16,17)
      write(16,9)  (fitrange(1,k), k=1,6)
      write(16,10) (fitrange(2,k), k=1,6)
      write(16,11) (fitrange(3,k), k=1,6)
      write(16,12) (fitrange(4,k), k=1,6)
      write(16,13) (fitrange(5,k), k=1,6)
      write(16,14) (fitrange(6,k), k=1,6)


      close(16)
      stop
    1 format('satellite 1 center x,y,z')
    2 format('satellite 2 center x,y,z')
```

```
    3 format('satellite 3 center x,y,z')
    4 format(' SPECIFIED POSITION:'/
     .       '             X           Y           Z')
    5 format(' SAT 1', 3f12.6)
    6 format(' SAT 2', 3f12.6)
    7 format(' SAT 3', 3f12.6)
    8 format(/' EXACT RANGES:'/
     .    '           top1        bot1',
     .       '        top2        bot2',
     .       '        top3        bot3')
    9 format(' top1', 6f12.6)
   10 format(' bot1', 6f12.6)
   11 format(' top2', 6f12.6)
   12 format(' bot2', 6f12.6)
   13 format(' top3', 6f12.6)
   14 format(' bot3', 6f12.6)
   15 format(/' PHASE-DERIVED RANGES:'/
     .    '           top1        bot1',
     .       '        top2        bot2',
     .       '        top3        bot3')
   16 format(/' NLLS-DERIVED POSITION:'/
     .       '             X           Y           Z')
   17 format(/' NLLS-DERIVED RANGES:'/
     .    '           top1        bot1',
     .       '        top2        bot2',
     .       '        top3        bot3')
      END


      subroutine fcn_pos(m,n,x,fvec,iflag)
************************************
* external function for lmdif fitting
************************************
      implicit real*8 (a-h,o-z)
      common/drcos/range(6,6)
      integer m,n,iflag
      dimension x(n),fvec(m)
      k = 0
************************************************
* satellite 1, antenna 1 - 1:3, 1:4, 1:5, 1:6
* 1, 3, 5 are top antennas; 2, 4, 6 are bottoms
************************************************
      k = k + 1
      fvec(k) = dsqrt( (x(4)       -  x(1)     )**2 +
     c                 (x(5)       -  x(2)     )**2 +
     c                 ((x(6)+3.5) - (x(3)+3.5))**2 )
      fvec(k) = fvec(k) - range(1,3)

      k = k + 1
      fvec(k) = dsqrt( (x(4)       -  x(1)     )**2 +
     c                 (x(5)       -  x(2)     )**2 +
     c                 ((x(6)-3.5) - (x(3)+3.5))**2 )
      fvec(k) = fvec(k) - range(1,4)

      k = k + 1
      fvec(k) = dsqrt( (x(7)       -  x(1)     )**2 +
     c                 (x(8)       -  x(2)     )**2 +
     c                 ((x(9)+3.5) - (x(3)+3.5))**2 )
      fvec(k) = fvec(k) - range(1,5)

      k = k + 1
      fvec(k) = dsqrt( (x(7)       -  x(1)     )**2 +
     c                 (x(8)       -  x(2)     )**2 +
     c                 ((x(9)-3.5) - (x(3)+3.5))**2 )
      fvec(k) = fvec(k) - range(1,6)

************************
* satellite 1, antenna 2 - 2:3, 2:4, 2:5, 2:6
************************
      k = k + 1
      fvec(k) = dsqrt( (x(4)       -  x(1)     )**2 +
```

```
     .                 (x(5)       -  x(2)     )**2 +
     .                 ((x(6)+3.5) - (x(3)-3.5))**2 )
      fvec(k) = fvec(k) - range(2,3)

      k = k + 1
      fvec(k) = dsqrt( (x(4)       -  x(1)     )**2 +
     .                 (x(5)       -  x(2)     )**2 +
     .                 ((x(6)-3.5) - (x(3)-3.5))**2 )
      fvec(k) = fvec(k) - range(2,4)

      k = k + 1
      fvec(k) = dsqrt( (x(7)       -  x(1)     )**2 +
     .                 (x(8)       -  x(2)     )**2 +
     .                 ((x(9)+3.5) - (x(3)-3.5))**2 )
      fvec(k) = fvec(k) - range(2,5)

      k = k + 1
      fvec(k) = dsqrt( (x(7)       -  x(1)     )**2 +
     .                 (x(8)       -  x(2)     )**2 +
     .                 ((x(9)-3.5) - (x(3)-3.5))**2 )
      fvec(k) = fvec(k) - range(2,6)

*************************
* satellite 2, antenna 1 - 3:1, 3:2, 3:5, 3:6
*************************
      k = k + 1
      fvec(k) = dsqrt( (x(1)       -  x(4)     )**2 +
     .                 (x(2)       -  x(5)     )**2 +
     .                ((x(3)+3.5)  - (x(6)+3.5))**2 )
      fvec(k) = fvec(k) - range(3,1)

      k = k + 1
      fvec(k) = sqrt(  (x(1)       -  x(4)     )**2 +
     .                 (x(2)       -  x(5)     )**2 +
     .                ((x(3)-3.5)  - (x(6)+3.5))**2 )
      fvec(k) = fvec(k) - range(3,2)

      k = k + 1
      fvec(k) = sqrt( (x(7)       -  x(4)     )**2 +
     .                 (x(8)       -  x(5)     )**2 +
     .                ((x(9)+3.5)  - (x(6)+3.5))**2 )
      fvec(k) = fvec(k) - range(3,5)

      k = k + 1
      fvec(k) = sqrt( (x(7)       -  x(4)     )**2 +
     .                 (x(8)       -  x(5)     )**2 +
     .                ((x(9)-3.5)  - (x(6)+3.5))**2 )
      fvec(k) = fvec(k) - range(3,6)

*************************
* satellite 2, antenna 2 - 4:1, 4:2, 4:5, 4:6
*************************
      k = k + 1
      fvec(k) = dsqrt( (x(1)       -  x(4)     )**2 +
     .                 (x(2)       -  x(5)     )**2 +
     .                ((x(3)+3.5) - (x(6)-3.5))**2 )
      fvec(k) = fvec(k) - range(4,1)

      k = k + 1
      fvec(k) = dsqrt( (x(1)       -  x(4)     )**2 +
     .                 (x(2)       -  x(5)     )**2 +
     .                ((x(3)-3.5)  - (x(6)-3.5))**2 )
      fvec(k) = fvec(k) - range(4,2)

      k = k + 1
      fvec(k) = dsqrt( (x(7)       -  x(4)     )**2 +
     .                 (x(8)       -  x(5)     )**2 +
     .                 ((x(9)+3.5) - (x(6)-3.5))**2 )
      fvec(k) = fvec(k) - range(4,5)

      k = k + 1
```

```
      fvec(k) = dsqrt( (x(7)       -  x(4)     )**2 +
     .                 (x(8)       -  x(5)     )**2 +
     .                 ((x(9)-3.5) - (x(6)-3.5))**2 )
      fvec(k) = fvec(k) - range(4,6)

*************************
* satellite 3, antenna 1 - 5:1, 5:2, 5:3, 5:4
*************************
      k = k + 1
      fvec(k) = dsqrt( (x(1)       -  x(7)     )**2 +
     .                 (x(2)       -  x(8)     )**2 +
     .                ((x(3)+3.5)  - (x(9)+3.5))**2 )
      fvec(k) = fvec(k) - range(5,1)

      k = k + 1
      fvec(k) = dsqrt( (x(1)       -  x(7)     )**2 +
     .                 (x(2)       -  x(8)     )**2 +
     .                ((x(3)-3.5)  - (x(9)+3.5))**2 )
      fvec(k) = fvec(k) - range(5,2)

      k = k + 1
      fvec(k) = dsqrt( (x(4)       -  x(7)     )**2 +
     .                 (x(5)       -  x(8)     )**2 +
     .                ((x(6)+3.5)  - (x(9)+3.5))**2 )
      fvec(k) = fvec(k) - range(5,3)

      k = k + 1
      fvec(k) = dsqrt( (x(4)       -  x(7)     )**2 +
     .                 (x(5)       -  x(8)     )**2 +
     .                ((x(6)-3.5)  - (x(9)+3.5))**2 )
      fvec(k) = fvec(k) - range(5,4)

*************************
* satellite 3, antenna 2 - 6:1, 6:2, 6:3, 6:4
*************************
      k = k + 1
      fvec(k) = dsqrt( (x(1)       -  x(7)     )**2 +
     .                 (x(2)       -  x(8)     )**2 +
     .                ((x(3)+3.5) - (x(9)-3.5))**2 )
      fvec(k) = fvec(k) - range(6,1)

      k = k + 1
      fvec(k) = dsqrt( (x(1)       -  x(7)     )**2 +
     .                 (x(2)       -  x(8)     )**2 +
     .                ((x(3)-3.5)  - (x(9)-3.5))**2 )
      fvec(k) = fvec(k) - range(6,2)

      k = k + 1
      fvec(k) = dsqrt( (x(4)       -  x(7)     )**2 +
     .                 (x(5)       -  x(8)     )**2 +
     .                ((x(6)+3.5)  - (x(9)-3.5))**2 )
      fvec(k) = fvec(k) - range(6,3)

      k = k + 1
      fvec(k) = dsqrt( (x(4)       -  x(7)     )**2 +
     .                 (x(5)       -  x(8)     )**2 +
     .                ((x(6)-3.5)  - (x(9)-3.5))**2 )
      fvec(k) = fvec(k) - range(6,4)

 3000 return
      end
```